Pinning of Texture and Vortices of the Rotating *B*-like Phase of Superfluid ^{3}He Confined in a 98% Aerogel

M. Yamashita,[2] A. Matsubara,[2,4] R. Ishiguro,[2,*] Y. Sasaki,[2,4] Y. Kataoka,[1] M. Kubota,[1] O. Ishikawa,[1,3] Yu. M. Bunkov,[6] T. Ohmi,[2] T. Takagi,[5] and T. Mizusaki[2,4]

[1]*Institute for Solid State Physics, The University of Tokyo, Chiba 277-8581, Japan*
[2]*Department of Physics, Graduate School of Science, Kyoto University, Kyoto 606-8502, Japan*
[3]*Graduate School of Science, Osaka City University, Osaka 558-8585, Japan*
[4]*Research Center for Low Temperature and Materials Sciences, Kyoto University, Kyoto 606-8502, Japan*
[5]*Department of Applied Physics, Fukui University, Fukui 910-8507, Japan*
[6]*CRTBT, CNRS, BP 166, 38042 Grenoble Cedex 9, France*

(Received 18 June 2004; published 22 February 2005)

We have investigated pinning effects on texture and vortices of the *B*-like phase of superfluid ^{3}He in a rotating aerogel up to $\pm 2\pi$ rad/s by cw-NMR. We observed deformation of the NMR spectra in rotation, due to counterflow between the superflow and the normal flow. The average intensity of the counterflow was calculated from the change of NMR spectra. The rotation dependence of the counterflow intensity is similar to the magnetization curve of hard type II superconductors or the counterflow response of ^{4}He-II in packed powders. This counterflow behavior is in qualitative agreement with a model that vortices are pinned unless the counterflow exceeds a critical velocity v_c. The temperature independence of v_c suggests that v_c is associated with the expansion of primordial vortices.

DOI: 10.1103/PhysRevLett.94.075301 PACS numbers: 67.57.Fg, 47.32.Cc, 67.57.Pq

Superfluid ^{3}He is known as the system in which the order parameter has many degrees of freedom, some of which are the order parameter vectors. A continuous spatial configuration of the order parameter (''texture'') has been widely investigated especially in the context of quantized vortices in rotation [1]. The discovery of superfluid ^{3}He in aerogel [2] provides us with a new possibility to study impurity effects. The superfluidity in aerogel has been extensively investigated [3], and theoretical calculations [4] for superfluid ^{3}He in aerogel show that it is not successful to treat the system as having a homogeneous impurity density, and it is necessary to account for the inhomogeneity of the impurity density. Such an inhomogeneity will modify the texture and provide pinning centers for the vortex in aerogel. The purpose of our experiment is to reveal these inhomogeneous effects on the texture and vortices by NMR measurements.

Measurements were performed by cw-NMR at the Larmor frequency $f_L = 700$ kHz under a pressure 3.0 MPa. We used a 98% porosity silica aerogel which has a cylindrical shape of radius $R = 2.6$ mm [5]. This aerogel was inserted into the cylindrical sample cell of Stycast 1266 with a very small clearance between the walls. The NMR field of $H = 22$ mT was applied parallel to the axis of the sample and that of a rotating cryostat at Institute for Solid State Physics [6], which could rotate at angular velocity $|\Omega| \leq 6.28$ rad/s. We have observed an *A*-like phase with a suppressed transition temperature $T_c = 2.05$ mK and a *B*-like phase below $0.85T_c$ on cooling and also observed the change of NMR spectra by rotation in the *B*-like phase, but not in the *A*-like phase [7]. In this Letter, we discuss the results in the rotating *B*-like phase in detail.

The NMR spectra at rest and in rotation at $0.59T_c$ are shown in Figs. 1(a) in acceleration and in Fig. 1(b) in deceleration, where the sample was cooled without rotation at T_c. The NMR spectrum at rest does not have a sharp frequency distribution as that in bulk liquid [8,9], but has a similar spectrum, especially a tail that extends towards the high frequency edge, $\Delta f_0 = 5.5$ kHz, as illustrated in Fig. 1(a). In the first acceleration, the NMR spectrum did not change below 1.0 rad/s. However, above 1.0 rad/s, the absorption in higher frequencies increased and that in lower frequencies decreased simultaneously [2–4 rad/s in Fig. 1(a)]. The change of absorption showed saturation under further acceleration. In deceleration from 6.28 rad/s, the spectrum changed in an inverse way [5.5 rad/s in Fig. 1(b)] and at 4–3 rad/s the spectrum was almost the same as that taken before the rotation. In further deceleration, the increase in the higher frequencies and the decrease in lower frequencies occurred again [below 2 rad/s in Fig. 1(b)]. Such a spectrum remained at 0 rad/s. The integral of the whole NMR spectra was independent of the rotation speed.

The similar change of the NMR spectra in acceleration has been observed in the vortex-free *B* phase in bulk liquid [8,9], which is caused by the orientational effect on $\hat{\boldsymbol{n}}$ by the counterflow between the normal flow $\boldsymbol{v}_n$ and the superflow $\boldsymbol{v}_s$, where $\hat{\boldsymbol{n}}$ is a vector characterizing the order parameter in ^{3}He-*B* [10]. When the sample cell is rotated, $\boldsymbol{v}_n$ flows as the solid body rotation $\boldsymbol{v}_n = v_n\hat{\varphi} = r\Omega\hat{\varphi}$, where r is the distance from the center and $\hat{\varphi}$ is an azimuthal unit vector. On the other hand, $\boldsymbol{v}_s = v_s\hat{\varphi}$ remains at rest at velocities less than a critical velocity needed for a vortex nucleation. The counterflow $\boldsymbol{v}_n - \boldsymbol{v}_s$

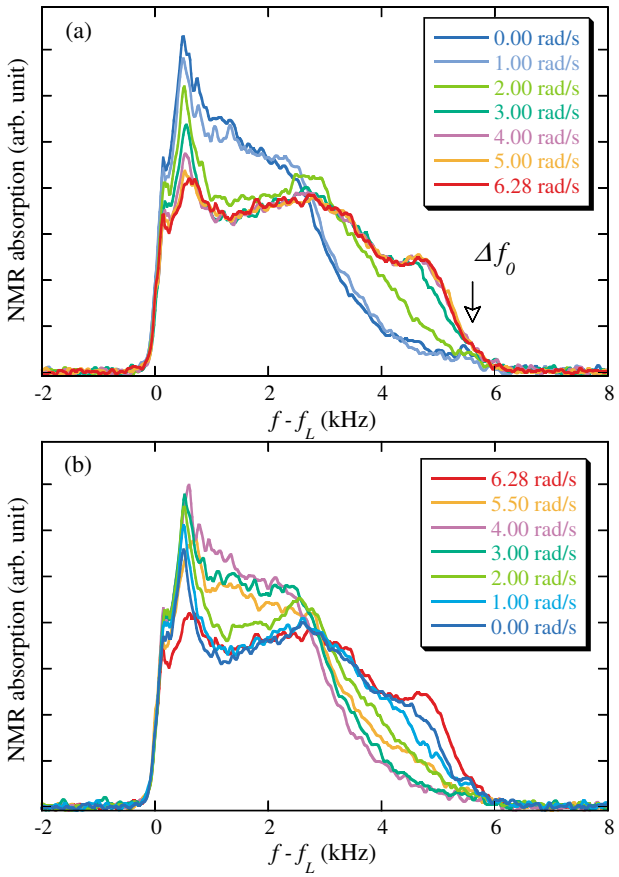

FIG. 1 (color). Rotation dependence of NMR spectra at $T = 0.59T_c$ in acceleration (a) and in deceleration (b).

tends to increase the angle $\beta(r, \Omega)$ between $\boldsymbol{H}$ and $\hat{\boldsymbol{n}}$ for $|v_n - v_s| \geq v_d$ as

$$\sin^2\beta(r, \Omega) = \frac{4}{5}\left(1 - \frac{v_d^2}{|v_n(r, \Omega) - v_s(r, \Omega)|^2}\right), \quad (1)$$

but for $|v_n - v_s| < v_d$, $\beta(r, \Omega) = 0$, where v_d is a characteristic speed [11]. The NMR absorption frequency $f(r, \Omega)$ in ^{3}He-B is given as

$$f(r, \Omega) = f_L + (f_B^2/2f_L)\sin^2\beta(r, \Omega) \quad (2)$$

for $f_L \gg f_B$, where f_B is the longitudinal frequency in the B phase in bulk liquid. From Eqs. (1) and (2), one can see that the NMR signal broadens towards higher frequency for $|v_n - v_s| > v_d$. Recently the B-like phase in aerogel has been confirmed to be analogous to the B phase in bulk ^{3}He [12,13]. Therefore, we can approximate about the B-like phase as having the same order parameter $\hat{\boldsymbol{n}}$ as in bulk liquid. We suggest that the change in absorption signal in aerogel by rotation can be attributed to changes of $\beta(r, \Omega)$ by the counterflow as in bulk liquid, where we assume that the angle β is a function of r and Ω over macroscopic length scale in aerogel. We attribute the broadened NMR spectrum at rest to a pinning of a part of $\hat{\boldsymbol{n}}$. However, to explain the change of the NMR spectra under rotation, we assume that the other part of $\hat{\boldsymbol{n}}$ remaining unpinned can move by the counterflow according to Eq. (1) and produce the deformation of the NMR spectra under rotation as in Fig. 1 [14].

From Eqs. (1) and (2), we can estimate $|v_n(r, \Omega) - v_s(r, \Omega)|/v_d$ from $f(r, \Omega)$ as $|v_n(r, \Omega) - v_s(r, \Omega)|/v_d = 1/\sqrt{1 - [f(r, \Omega) - f_L]/\Delta f_0}$ for $|v_n(r, \Omega) - v_s(r, \Omega)| \geq v_d$, where we determined the longitudinal frequency in aerogel, f_B^{aero}, by choosing Δf_0 as the extrapolated end point of the envelope of the NMR spectrum and using $\Delta f_0 = 0.4(f_B^{\mathrm{aero}})^2/f_L$ as in the bulk liquid [8]. In the local oscillation approximation, the NMR spectrum is directly related to $f(r, \Omega)$ such that the absorption intensity $I(f, \Omega)$ is proportional to $\int_0^R \delta(f - f(r, \Omega))2\pi r dr$. Therefore, one finds the integration of

$$F_1(\Omega) \equiv \frac{1}{I_{\mathrm{total}}} \int_{f_L}^{f_L + \Delta f_0} \frac{I(f, \Omega)}{\sqrt{1 - (f - f_L)/\Delta f_0}} df \quad (3)$$

is equal to the average intensity of the counterflow of

$$F_1(\Omega) = \frac{1}{\pi R^2} \int_0^R \frac{|v_n(r, \Omega) - v_s(r, \Omega)|}{v_d} 2\pi r dr \quad (4)$$

for $|v_n - v_s| \geq v_d$, where $I_{\mathrm{total}} = \int_{f_L}^{f_L + \Delta f_0} I(f, \Omega) df$. To eliminate the broadening effect on the NMR spectrum at rest, we calculate the difference of $F_1(\Omega)$ from the value before rotation, $F_1(0)$, as $\Delta F_1(\Omega) = F_1(\Omega) - F_1(0)$. A result of the calculation of $\Delta F_1(\Omega)$ by using Eq. (3) is plotted as a function of Ω in Fig. 2, where we changed Ω by successive steps of 0.1 rad/s at $0.59T_c$ and obtained a series of NMR spectra.

As shown in Fig. 2, there was no change in $\Delta F_1(\Omega)$ in the first stage in acceleration below $\Omega_d = 1.0$ rad/s. For $\Omega_d < \Omega < \Omega_c$, $\Delta F_1(\Omega)$ increased almost linearly with Ω (solid line in Fig. 2). We assume that there is no v_s below Ω_c in the first acceleration after cooling at rest. Thus the linear increase of $\Delta F_1(\Omega)$ can be explained by the deformation of $\hat{\boldsymbol{n}}$ by v_n, and the no change of $\Delta F_1(\Omega)$ is attributed to the insensitivity of $\hat{\boldsymbol{n}}$ for $v_n < v_d$. This consideration is consistent with Eq. (4). When the rotation speed exceeded $\Omega_c = 2.7$ rad/s, $\Delta F_1(\Omega)$ deviated from the linear behavior. This deviation is attributed to the increase of v_s by vortices.

In deceleration, $\Delta F_1(\Omega)$ decreased and reached a minimum at $|\Omega| = \Omega_v \sim 3.8$ rad/s, where $|v_n - v_s|$ in the whole sample became less than v_d. Under further deceleration, $\Delta F_1(\Omega)$ increased again and a large intensity remained even at $\Omega = 0$. We conclude that this large $\Delta F_1(0)$ after the rotation is due to a finite v_s by pinned vortices in aerogel. This hysteresis was observed once the rotation speed exceeded Ω_c. If the rotation speed was kept less than Ω_c, $\Delta F_1(\Omega)$ showed no hysteresis. No decay of the superflow at $\Omega = 0$ was observed within 40 h.

The calculated result of Eq. (3) does not show v_n below Ω_d due to the insensitivity of $\hat{\boldsymbol{n}}$ for $|v_n - v_s| < v_d$. Since

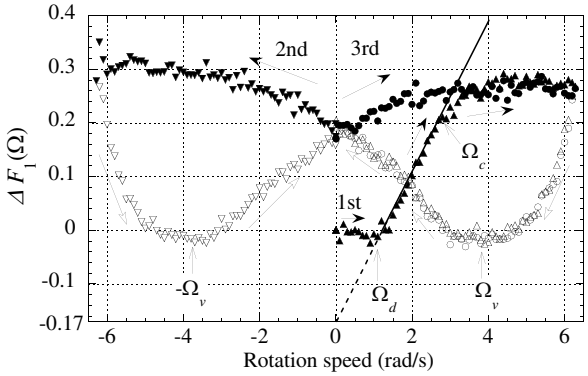

FIG. 2. Rotation dependence of the average intensity of the counterflow at $T = 0.59T_c$. Three runs are represented as 1st (▲, △), 2nd (▼, ▽), and 3rd (●, ○). The filled symbols and open ones correspond to data in acceleration and that in deceleration, respectively. $\Omega_d = 1.0$ rad/s is the onset of the texture deformation due to the counterflow, $\Omega_c = 2.7$ rad/s is the critical velocity of the vortex penetration into the aerogel, and $\pm\Omega_v = \pm 3.8$ rad/s where the counterflow in the whole sample is less than v_d. The solid line is a guide for the eye to show the linear behavior for $\Omega_d < \Omega < \Omega_c$, and the broken line is an extrapolation of the solid line.

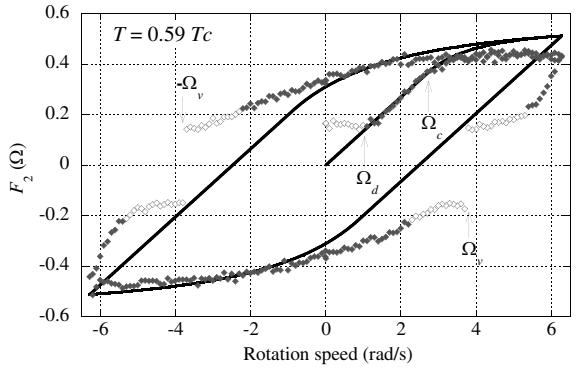

FIG. 3. Integral of the counterflow in the aerogel obtained with the procedure in the text. The solid line shows a result of the calculation of $F_2(\Omega)$ based on the vortex pinning model shown in Fig. 4. We plot the data for $\Omega < \Omega_d$ in the first acceleration and near $\pm\Omega_v$ in deceleration as open symbols to show that these data do not correspond to $F_2(\Omega)$ due to the insensitivity of $\hat{\boldsymbol{n}}$ for $|v_n - v_s| < v_d$.

we assume that there is no v_s below Ω_c, we can take into account a finite v_d effect by shifting the data in Fig. 2 by $+0.17$ so that the linear behavior of $\Delta F_1(\Omega)$ for $\Omega_d < \Omega < \Omega_c$ passes through the origin (broken line in Fig. 2). Also, we assume that the direction of v_s remains unchanged in deceleration below Ω_v and that the sign of $\int_0^R (v_n - v_s) 2\pi r dr$ changes at Ω_v. To show the counterflow direction, we inverted the signs of the shifted $\Delta F_1(\Omega)$ at $\pm\Omega_v$ in deceleration [see Eq. (4)]. With this procedure, we obtained the modified result in Fig. 3. These data except for $\Omega < \Omega_d$ in the first acceleration and near $\pm\Omega_v$ in deceleration correspond to the integral of counterflow at each Ω,

$$F_2(\Omega) = \frac{1}{\pi R^2} \int_0^R \frac{v_n(r,\Omega) - v_s(r,\Omega)}{v_d} 2\pi r dr, \quad (5)$$

where we approximate v_s as the average superflow. It is clear that the magnetization curve of hard type II superconductors [15] and the superflow curve of superfluid ^{4}He in packed powders [16] are very similar to $F_2(\Omega)$ in Fig. 3.

From the structure of aerogel, we expect that there are so many pinning centers for vortices in aerogel that vortices cannot move freely as in bulk liquid, and that vortices need a critical velocity v_c to change their distribution in aerogel. In Fig. 4, we propose velocity profiles of our vortex pinning model to visualize the counterflow in aerogel. In acceleration, vortices can penetrate into the aerogel sample only where $|v_n(r) - v_s(r)| > v_c$. The counterflow cannot become lower than v_c because vortices need a counterflow larger than v_c to move in aerogel. As a result, the counterflow remains at a constant, v_c, in the vortex region as illustrated in Figs. 4(b)–4(d). The observed Ω_c in Fig. 2 is related to v_c as $v_c = R\Omega_c$. In deceleration, the vortices are pinned and do not move for $|v_n(r) - v_s(r)| < v_c$ [Fig. 4(e)]. However, v_n is reduced, causing the decrease of $|v_n(r) - v_s(r)|$ in the whole sample. In further deceleration v_n becomes smaller than the trapped v_s and $|v_n(r) - v_s(r)|$ increased again. For $v_n(r) - v_s(r) < -v_c$ [Figs. 4(f)–4(h)], the vortices start to move outward in aerogel and vortices with an opposite circulation start to

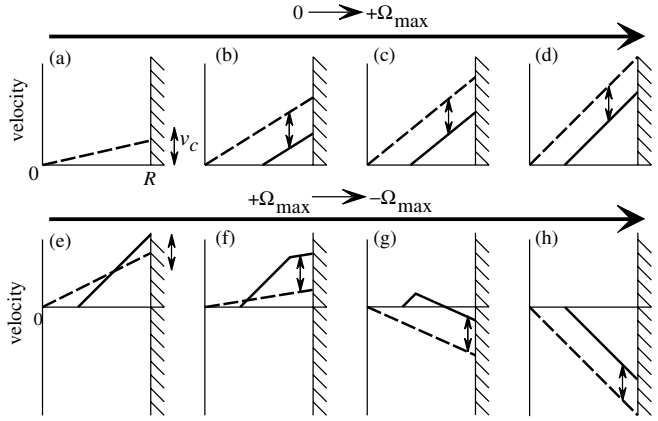

FIG. 4. Velocity profiles in aerogel used for calculating $F_2(\Omega)$ in Fig. 3 for $0 \rightarrow +\Omega_{max} = 6.28$ rad/s (a)–(d), and for $+\Omega_{max} \rightarrow -\Omega_{max}$ (e)–(h). The radial distribution of velocity of normal flow (dashed lines) and averaged superflow (solid lines) are illustrated. The length of the arrow represents the magnitude of v_c. (a) $\Omega < \Omega_c$, there is no vortex inside the aerogel. (b),(c) $\Omega > \Omega_c$, vortices start to penetrate into the aerogel near the wall and the vortex region expands. (d) $\Omega = \Omega_{max}$. (e) At the start of the deceleration cycle, $\Omega > \Omega_{max} - 2\Omega_c$, vortices are pinned, and v_s remains unchanged. In (f),(g) $\Omega < \Omega_{max} - 2\Omega_c$, vortices start to redistribute and the opposite superflow appears. (h) $\Omega = -\Omega_{max}$.

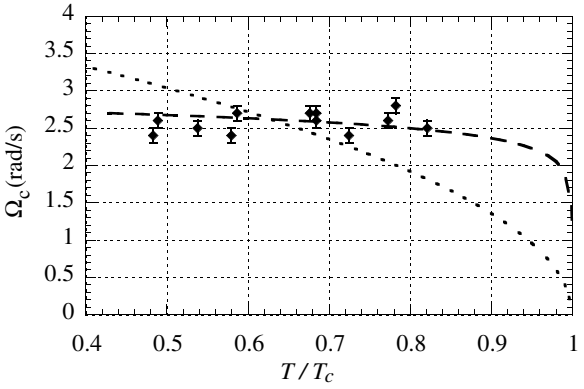

FIG. 5. Ω_c vs reduced temperature. The dashed line shows the result of Eq. (6) with $d = 10.5$ μm, and the dotted line shows a fitting curve when $v_c \propto \Delta(T) \propto \sqrt{1 - T/T_c}$.

penetrate into the aerogel so that v_s changes from the outside. The vortices with opposite circulations may disappear by recombination. By the velocity profiles in Fig. 4, we used Eq. (5) to fit the experimental data so that the calculated $F_2(\Omega)$ fits the data at Ω_c. The result of this calculation is plotted as the solid line in Fig. 3, which qualitatively describes most features of the observed data.

The essential difference between vortices in aerogel and those in bulk liquid is their distribution under rotation. We speculate that an inhomogeneity of the impurity density causes the energy gap Δ to be inhomogeneous and vortices are trapped at local minima of Δ. If v_c is associated with depinning of vortices from the trapping potential, v_c should have the same temperature dependence of $\Delta(T)$ as in bulk liquid [9]. However, the observed Ω_c was nearly independent of temperatures as shown in Fig. 5. Glaberson and Donnelly attribute the growth of pinned quantized vortex lines in superfluid ^{4}He as causing the onset of instability of superflow [17]. They assert that, when both ends of a vortex line are pinned, vortices can remain as the stable form for $|v_n - v_s| < v_c$ by the self-induced velocity. In analogy with their estimate, we consider that v_c above which a pinned vortex in aerogel becomes unstable is determined by the distance between the pinning points d as

$$v_c = \frac{\kappa}{2\pi d}\left[\ln\left(\frac{4d}{\xi(T)}\right) - \frac{1}{4}\right], \tag{6}$$

where $\xi(T)$ is the coherence length of ^{3}He-B. We think that there are some primordial vortices in aerogel and that, for $|v_n - v_s| > v_c$, these vortices start to expand and reconnect to make the vortex line shorter and produce another pinned vortex line at other pinning points. A plot of Eq. (6) for $d = 10.5$ μm is shown as the dashed line in Fig. 5, which is consistent with observed critical velocities though we cannot provide an explanation for the relatively large magnitude of $d = 10.5$ μm. We conclude that we have observed the growth and reconnection of primordial vortices, in response to the altered counterflow, to redistribute the density of pinned vortices. However, a more complete consideration is needed for further study.

In conclusion, we have obtained the rotation dependence of the integral of the counterflow in aerogel by NMR spectra. The hysteresis of the curve can be qualitatively explained by the vortex pinning model. The temperature dependence of the critical velocity for the penetration of vortices into aerogel is consistent with that of growth of primordial vortices whose ends are pinned.

M. Yamashita acknowledges the support of the JSPS. This work was carried out using facilities of the Institute for Solid State Physics, the University of Tokyo, and was partially supported by the Grant-in-Aid for Scientific Research from MEXT and by the Grand-in-Aid for the 21st Century COE "Center for Diversity and Universality in Physics."

*Current address: ENS, 24 rue Lhomond, 75231 Paris Cedex 05, France.

[1] E. R. Dobbs, *Helium Three* (Oxford University Press, New York, 2000).
[2] J. V. Porto and J. M. Parpia, Phys. Rev. Lett. **74**, 4667 (1995).
[3] W. P. Halperin *et al.*, Physica (Amsterdam) **329B–333B**, 288 (2003).
[4] R. Hänninen and E. V. Thuneberg, Phys. Rev. B **67**, 214507 (2003).
[5] This sample was used in experiments in Grenoble [Yu. M. Bunkov *et al.*, Phys. Rev. Lett. **85**, 3456 (2000)].
[6] M. Kubota *et al.*, Physica (Amsterdam) **329B–333**B, 1577 (2003).
[7] M. Yamashita *et al.*, J. Low Temp. Phys. **134**, 749 (2004).
[8] P. J. Hakonen *et al.*, J. Low Temp. Phys. **76**, 225 (1989).
[9] V. M. H. Ruutu *et al.*, J. Low Temp. Phys. **107**, 93 (1997).
[10] D. Vollhardt and P. Wölfle, *The Superfluid Phases of Helium 3* (Taylor & Francis, London, 1990).
[11] W. F. Brinkman and M. C. Cross, in *Progress in Low Temperature Physics*, edited by D. F. Brewer (North-Holland, Amsterdam, 1978), Vol. VIIa, p. 105.
[12] H. Alles *et al.*, Phys. Rev. Lett. **83**, 1367 (1999).
[13] V. V. Dmitriev *et al.*, JETP Lett. **76**, 312 (2002).
[14] A bulk contribution coming from outside the aerogel is negligible, because the bulk signal is estimated to be as small as 3% of the total NMR signal at the temperatures (see Fig. 1 of our previous paper [7]).
[15] C. P. Bean, Rev. Mod. Phys. **36**, 31 (1964).
[16] H. Kojima *et al.*, *Low Temperature Physics—LT-13*, edited by K. D. Timmershaus, W. J. O'Sullivan, and E. F. Hammel (Plenum, New York, 1974), Vol. 1, p. 279.
[17] W. I. Glaberson and R. J. Donnelly, Phys. Rev. **141**, 208 (1966).